

1 **Convergent loss of the necroptosis pathway in disparate mammalian**  
2 **lineages shapes virus countermeasures**

3

4 **Ana Águeda-Pinto<sup>a,b</sup>, Luís Q. Alves<sup>c</sup>, Fabiana Neves<sup>a</sup>, Grant McFadden<sup>d</sup>, Bertram L**  
5 **Jacobs<sup>d,e</sup>, L. Filipe C. Castro<sup>b,c</sup>, Masmudur M. Rahman<sup>d</sup> and Pedro J. Esteves<sup>a,b,f#</sup>**

6

7 <sup>a</sup>CIBIO/InBio-Centro de Investigação em Biodiversidade e Recursos Genéticos,  
8 Universidade do Porto, Vairão, Portugal

9 <sup>b</sup>Departamento de Biologia, Faculdade de Ciências, Universidade do Porto, Porto,  
10 Portugal

11 <sup>c</sup>CIIMAR/CIMAR, Centro Interdisciplinar de Investigação Marinha e Ambiental,  
12 Universidade do Porto, Matosinhos, Portugal

13 <sup>d</sup>Center for Immunotherapy, Vaccines and Virotherapy (CIVV), The Biodesign Institute,  
14 Arizona State University, Tempe, USA

15 <sup>e</sup>School of Life Sciences Center for Immunotherapy, Vaccines and Virotherapy, Biodesign  
16 Institute, Arizona State University, Tempe, USA

17 <sup>f</sup>CITS-Centro de Investigação em Tecnologias da Saúde, IPSN, CESPU, Gandra, Portugal

## 18 **Abstract**

19           Programmed cell death is a vital process in the life cycle of an organism.  
20 Necroptosis, an evolutionary restricted form of programmed necrosis, contributes to the  
21 innate immune response by killing pathogen-infected cells. This virus-host interaction  
22 pathway is organized around two key components: the receptor-interacting protein kinase  
23 3 (RIPK3), which recruits and phosphorylates the mixed lineage kinase-like protein  
24 (MLKL), thus inducing cellular plasma membrane rupture and cell death. Critically, the  
25 presence of necroptotic inhibitors in viral genomes validates necroptosis as an important  
26 host defense mechanism. Here, we show, counterintuitively, that in different mammalian  
27 lineages of mammalian, central components of the necroptotic pathway, such as *RIPK3*  
28 and *MLKL* genes, are deleted or display inactivating mutations. Frameshifts or premature  
29 stop codons are observed in all the studied species of cetaceans and leporids. In  
30 carnivores' genomes, the *MLKL* gene is deleted, while in a small number of species from  
31 afrotheria and rodentia premature stop codons are observed in *RIPK3* and/or *MLKL*.  
32 Interestingly, we also found a strong correlation between the disruption of necroptosis in  
33 leporids and cetaceans and the absence of the C-terminal domain of E3-like homologs  
34 (responsible for necroptosis inhibition) in their naturally infecting poxviruses. Overall, our  
35 study provides the first comprehensive picture of the molecular evolution of necroptosis in  
36 mammals. The loss of necroptosis multiple times during mammalian evolution highlights  
37 the importance of gene/pathway loss for species adaptation and suggests that necroptosis  
38 is not required for normal mammalian development. Moreover, this study highlights a co-  
39 evolutionary relationship between poxviruses and their hosts, emphasizing the role of host  
40 adaptation in shaping virus evolution.

## 41 Introduction

42 Sensing of viral pathogens by the host cells is critical for animal survival. Thus, a  
43 variety of molecular responses, including the induction of inflammatory cytokines,  
44 chemokines and interferons, as well as the activation of cell-death pathways that provide  
45 clearance of pathogen-infected cells. Although apoptosis has long been considered a  
46 critical clearance mechanism to control viral spread, caspase-independent cell death, or  
47 programmed necrosis, has recently emerged as an alternative death pathway that  
48 dominates under specific conditions (Xia et al. 2020).

49

50 Necroptosis is an inflammatory form of regulated necrosis that acts as an  
51 alternative host defense pathway during some viral infections and plays a major role in the  
52 killing and removal of pathogen-infected cells (Upton and Chan 2014; Nogusa et al. 2016;  
53 Xia et al. 2020). Activation of necroptosis follows an intracellular signaling cascade that is  
54 dependent on the receptor-interacting serine/threonine-protein kinase 3 (RIPK3) and its  
55 substrate, the mixed lineage kinase like protein (MLKL) downstream of death receptors  
56 (DRs) and pattern-recognition receptors (PPRs) (Fig. 1) (Sun et al. 2012; Moerke et al.  
57 2019). Several pathway-specific adaptor proteins that contain a RIP homotypic interaction  
58 motif (RHIM-domain) can activate RIPK3-induced necroptosis (Fig. 1). For example, when  
59 there is an interference or loss of function of caspase-8, the induction of necroptosis  
60 through the use of DRs results in the recruitment of RIPK1, which subsequently exposes  
61 its RHIM-domain to recruit RIPK3 (He et al. 2009; Zhang et al. 2009; Upton et al. 2010).  
62 Apart from RIPK1, the TIR-domain-containing adaptor-inducing IFN  $\beta$  (TRIF), an essential  
63 protein downstream of Toll-like receptor (TLR)3/4 and the Z-DNA binding protein (ZBP1),  
64 also directly activate RIPK3 (He et al. 2011; Upton et al. 2012) (Fig. 1). Exposure of RIPK3  
65 to a RHIM adaptor (RIPK1, TRIF or ZBP1) is a crucial step in the initiation of necroptosis,  
66 as these proteins activate the downstream executor of necroptosis MLKL that destabilizes  
67 the plasma membrane integrity leading to cell swelling followed by membrane rupture of  
68 infected cells and release of damage-associated molecular patterns (DAMPs) (Kaiser et al.  
69 2013; Upton and Chan 2014). Thus, necroptosis provides a critical extra defense  
70 mechanism against pathogen infection, facilitating the elimination of virus-infected cells  
71 before the production of progeny virions. The importance of necroptosis for host defense is  
72 further supported by the identification of viral inhibitors of necroptosis, like is the case of  
73 Vaccinia virus (VACV) E3 protein and the murine cytomegalovirus (MCMV) M45 protein  
74 (Upton et al. 2012; Kaiser et al. 2013).

75

76 Necroptosis has a major role in protecting cells against viral infection (Upton and  
77 Chan 2014; Nogusa et al. 2016; Xia et al. 2020). However, despite the recent advances to  
78 understand the molecular regulation of this unique pathway, it is still unclear whether the  
79 necroptotic cell death pathway acts as a universal cell death program in mammals.  
80 Previous studies suggested that components of necroptosis are absent in the genomes of  
81 extant birds and marsupials. Interestingly, within the Mammalia class, it was previously  
82 reported that order Carnivora lost the *MLKL* gene (Dondelinger et al. 2016). Taken  
83 together these reports suggest some degree of plasticity in the conservation of necroptosis  
84 responses. Here, we address the molecular evolution of the necroptotic pathway in  
85 multiple mammalian lineages. We show that during mammalian evolution, necroptosis was  
86 convergently inactivated several times in mammalian lineages. Remarkably, we also report  
87 that mammalian orders that lost the necroptotic pathway display infection episodes by  
88 poxviruses that have lost the ability to inhibit this pathway, showing a co-evolutionary  
89 relationship between host adaptation in shaping virus evolution.

## 90 **Results**

91 Necroptosis has a significant role in protecting cells against viral infection (Upton  
92 and Chan 2014; Nogusa et al. 2016; Xia et al. 2020). However, despite recent advances to  
93 understand the molecular regulation of this unique pathway, it is still unclear whether the  
94 necroptotic cell death pathway acts as a universal cell death program in mammals. Here,  
95 taking advantage of genomic collection databases and the use of Leporid samples (see  
96 Methods section for more information), the goal is to better understand the molecular  
97 evolution of the necroptotic pathway in different mammalian lineages.

98

### 99 **RIPK1 protein is under evolutionary conservation in mammals**

100 Human RIPK1 is a multidomain protein composed of an N-terminal Ser/Thr kinase,  
101 a C-terminal death binding domain that mediates binding to DRs and an intermediate  
102 domain that includes a K377 ubiquitination site and an RHIM motif that binds to other  
103 RHIM-containing proteins (He and Wang 2018). Due to the importance of RIPK1 as an  
104 adaptor molecule, previous phylogenetic analysis suggested that RIPK1 probably emerged  
105 in the ancestor of vertebrates (Dondelinger et al. 2016). In accordance, our search  
106 detected the presence of *RIPK1* homologues in all the studied mammalian lineages (Fig.  
107 2A and S Appendix 1, 2 and 3).

108

109 To look for evidence of potential selection pressures acting on the different  
110 domains of RIPK1 protein, we used the dataset of mammalian sequences mentioned  
111 above and implemented an ML approach, by using the Datamonkey software (see  
112 Methods section for more information). For most protein-coding genes, the rate between  
113 nonsynonymous and synonymous substitutions (dN/dS) is a measure of natural selection,  
114 with positive selection (dN/dS > 1) acting against the common genotype (Kosiol et al.  
115 2008). In this study, we deduced ten sites that reflect strong positive selection pressure in  
116 RIPK1, while more than 200 amino acids were under negative selection (Fig. 2B and S  
117 Appendix 4). As seen in Fig. 2B, residues identified as being under positive selection fall  
118 within or very close to the kinase domain (4 residues), the RHIM domain (5 residues) and  
119 the death domain (1 residue) of RIPK1 (residues under positive selection are marked as  
120 red circles). The N-terminal kinase domain is known to present several essential residues  
121 for phosphorylation and ubiquitination (Ser<sup>14/15</sup>, 20, 161 and 166 and Lys<sup>115</sup> and 163),  
122 regulation of necroptosis and RIPK1-dependent apoptosis (Mifflin et al. 2020).  
123 Interestingly, the codons under positive selection fall only at the end of the N-terminal

124 domain. A considerable portion of the negatively selected sites fall in the critical regions for  
125 phosphorylation and ubiquitination (S Appendix 4), suggesting that the beginning of the  
126 RIPK1 protein is under strong purifying selection. The same was also observed for the  
127 rapidly evolving sites of the RHIM domain, which were grouped only at the beginning of  
128 this domain (Fig. 2B). It was previously shown that the RHIM domain has a crucial  
129 conserved core motif of 12 amino acids that resides at the end of this domain (Sun et al.  
130 2002; Li et al. 2012). Indeed, changing four consecutive amino acids to alanine within this  
131 core region abrogates interaction between RHIM domains and, as a consequence,  
132 necroptosis (Sun et al. 2002; Li et al. 2012). Our findings that the positively selected  
133 residues did not overlap with the core motif of 12 amino acids further support the  
134 importance of the conservation of this region. Interestingly, in the RIPK1 death domain that  
135 is known to mediate homodimerization as well as heterodimerization with other DD-  
136 containing proteins, such as FADD, TNFR1 and Fas (Meng et al. 2018; Mifflin et al. 2020),  
137 no positively selected sites were found, with most of the domain being under negative  
138 pressure (S Appendix 4). Collectively, our results show signatures of positive selection  
139 occurring at the end of the N-terminal kinase domain and at the beginning of the RHIM  
140 domain of RIPK1 proteins. Interestingly, these residues do not overlap with domains  
141 known to be fundamental for RIPK1-dependent apoptosis and necroptosis, suggesting that  
142 these domains might be under evolutionary conservation and possibly functional constraint  
143 for the studied mammals.

144

#### 145 **Convergent erosion of RIPK3 and MLKL in mammalian lineages**

146 RIPK3 and MLKL form the core of the necroptotic machinery and both are, as a  
147 consequence, important for necroptosis induction in mice and humans downstream of  
148 PRRs and DRs (Sun et al. 2012; Moerke et al. 2019; Xia et al. 2020). To further  
149 understand the evolutionary history of the necroptotic pathway in mammals, we performed  
150 detailed sequence and phylogenetic analyses for RIPK3 and MLKL homologous proteins  
151 (S Appendix 3). Our screens for *RIPK3* and *MLKL* genes revealed evidence of  
152 pseudogenization in five mammalian lineages: order rodentia, lagomorpha, carnivora,  
153 cetacean and in the superorder afrotheria (Fig. 2A). Given the fact that *MLKL*  
154 pseudogenes have been previously identified in carnivores, they will not be discussed in  
155 detail here (Dondelinger et al. 2016).

156

## 157 **Variation of the Necroptotic pathway within Afrotherian and Rodent families**

158 In afrotherian and rodent lineages, we found that the necroptotic pathway was  
159 missing in some species (Fig. 2A). In rodents, two species from the Bathyergidae family  
160 and one species from the Octodontidae family presented early stop codons in both RIPK3  
161 and MLKL, resulting in the disruption of necroptosis. In the naked mole-rat  
162 (*Heterocephalus glaber*), RIPK3 presented a premature stop codon in exon 6 resulting in a  
163 shorter version of this protein (S Appendix 5). In the common degu (*Octodon degus*) and  
164 in the damaraland mole-rat (*Fukomys damarensis*), both RIPK3 and MLKL proteins  
165 presented several premature stop codons (S Appendix 5). However, disruption of these  
166 proteins appears to have occurred in an independent way, rather than in a common  
167 ancestral. Given the fact that *RIPK3* and *MLKL* present signs of pseudogenization, it is  
168 expected that in the naked mole-rat, common degu and damaraland mole-rat necroptosis  
169 is disrupted. Our studies also revealed that species from Afrotherian families, including the  
170 African bush elephant (*Loxodonta africana*, family Elephantidae) and the Cape golden  
171 mole (*Chrysochloris asiatica*, family Chrysochloridae) presented early stop codons in  
172 RIPK3 and MLKL, respectively, while the the West Indian manatee (*Trichechus manatus*,  
173 family Trichechidae) present early stop codons in both genes (S Appendix 5). However,  
174 our results also show that the Cape elephant (*Elephantulus edwardii*, family  
175 Macroscelididae) and the lesser hedgehog tenrec (*Echinops telfairi*, family Tenrecidae)  
176 present intact copies of the *RIPK3* and *MLKL* genes, indicating that RIPK3 and MLKL were  
177 present in early stages of Afrotheria evolution, but must have been lost later in specific  
178 lineages, resulting in the existence of alternative modes of necroptosis inactivation.

179

## 180 **The Necroptotic pathway is disrupted in Lagomorphs**

181 The Order Lagomorpha is divided into two families, Ochotonidae and Leporidae,  
182 which diverged around 30–35 Mya (Melo-Ferreira et al. 2015). While Ochotonidae is only  
183 composed of one extant genus, *Ochotona*, the Leporidae family includes 11 genera,  
184 including *Lepus*, *Sylvilagus* and *Oryctolagus* (Ge et al. 2013). Using the methods  
185 described previously, we were only able to identify *RIPK3* and *MLKL* transcripts for plateau  
186 Pika (*O. curzoniae*), while no *RIPK3* and *MLKL* transcripts were found for the European  
187 rabbit (*O. cuniculus*). For the American Pika (*O. princeps*), incomplete genome assemblies  
188 in the vicinity of the *RIPK3* and *MLKL* regions made retrieving the sequence of these  
189 genes impossible. By evaluating *RIPK3* gene from human and mouse and its genomic  
190 context, we were able derive a partial *RIPK3* nucleotide sequence from the European

191 rabbit genome, which displays a frameshift mutation caused by the insertion of a single  
192 nucleotide. It is well known that accurately detecting gene-inactivation mutations in these  
193 alignments poses a number of challenges like, for example, sequencing errors and cases  
194 of assembly incompleteness. For this reason, we assessed the accuracy of our database  
195 prediction by sequencing that same genomic region in different Leporid species,  
196 representative of different genera (*Lepus*, *Sylvilagus* and *Oryctolagus*). From the obtained  
197 results, we confirmed the insertion of 1 nucleotide (+G, exon 3) not only in the European  
198 rabbit *RIPK3*, but also in species from genus *Lepus* and *Sylvilagus*, suggesting that  
199 disruption of *RIPK3* gene occurred in a common ancestral and was maintained throughout  
200 Leporid evolution (Fig. 3A). During necroptosis, activated *RIPK3* phosphorylates and  
201 activates *MLKL*, which results in its recruitment and oligomerization in the plasma  
202 membrane leading to rupture and cell death (Sun et al. 2012; Xia et al. 2020).  
203 Interestingly, and despite all of our efforts, no *MLKL* transcripts or *MLKL* protein  
204 accumulation were found in any of the studied Lagomorphs (data not shown). Detailed  
205 analysis of the upstream and downstream *MLKL* flanking genes in both human and mouse  
206 genomes reveal that *MLKL* resides between the ring finger and WD repeat domain 3  
207 protein (*RFWD3*) and fatty acid 2-hydroxylase (*FA2H*) genes (Fig. 4). Accordingly,  
208 although there are no gaps or incomplete genomic assemblies surrounding that region in  
209 the European rabbit genome, we were not able to retrieve a complete or partial *MLKL*  
210 gene, suggesting once more that this gene is not present in these mammals. Together, our  
211 results suggest that the studied leporid species are deficient in the core proteins of the  
212 necroptotic pathway, and that *RIPK3* inactivation occurred at the stem Leporid branch and  
213 was maintained during evolution.

214

### 215 **Inactivation of necroptosis components in Cetacea**

216 Modern Cetacea comprises Mysticete (or baleen whales) and Odontocete (or  
217 toothed whales) and are the most specialized and diversified group of mammals  
218 (McGowen et al. 2020). Comparative analysis of cetacean genomes has already provided  
219 important insights into the unique cetacean traits and aquatic specializations (Sharma et  
220 al. 2018; Huelsmann et al. 2019; Kawasaki et al. 2020). For our screen, Odontocetes were  
221 represented by 12 species belonging to five different families (Delphinidae, Phocoenidae,  
222 Monodontidae, Lipotidae and Physteridae), and Mysticetes were represented by the  
223 common minke whale from Balaenopteridae family. In Cetacean species, the disruption of  
224 *RIPK3* occurred at different positions depending on the studied species: a frameshift



225 mutation was identified in exon 6 of two Delphinidae species, as well as in exon 8 of two  
226 Phocoenidae species, one Monodontidae species and one Balaenopteridae species.  
227 There was also evidence of two species (one species from Monodontidae and another  
228 from Lipotidae families) with RIPK3 pseudogenes based on the presence of a stop codon  
229 located in exon 2 (S Appendix 6). Interestingly, while Cetacean RIPK3 inactivation appears  
230 to be a result of different mutations depending on the studied species, our results show a  
231 shared mutation in the exon 1 of *MLKL* in all cetacean species (Fig. 3B). Moreover, this  
232 premature stop codon leads to the absence of exon 2, 3, 4 and 5 in most cetacean  
233 species, which very likely results in this gene inactivation. Given the presence of an  
234 inactivating mutation that is shared between mysticetes and odontocetes, the most  
235 parsimonious hypothesis suggests that they occurred before the split of these two clades  
236 in the common ancestral branch of Cetacea.

237

### 238 **Diversity among the poxvirus encoded E3-like necroptosis antagonists**

239 Previously, it was shown that the N-terminus of VACV E3 competes with ZBP1 for  
240 binding to virus-induced Z-nucleic acid, being a key component to inhibit the action of IFN  
241 and induction of necroptosis (Koehler et al. 2017) (Fig. 1). E3-like encoded proteins are  
242 composed of a carboxy (C)-terminal double-stranded RNA binding domain (dsRNA-BD)  
243 and an amino (N)-terminal Z-nucleic acid-binding domain (zNA-BD) (Kim et al. 2003; Kim  
244 et al. 2004) (Fig. 5A). Given the importance of the N-terminus region from VACV E3  
245 protein against virus infection, we hypothesize that poxviruses that lack this region in their  
246 E3 homologs can still successfully replicate in their natural host because of a  
247 compromised necroptotic pathway. Among the E3L proteins, E3 from VACV is the best  
248 studied protein. However, E3 homologs can be found in orthopoxviruses, clade II  
249 poxviruses and parapoxviruses (Kim et al. 2003; Kim et al. 2004). Recently, the genome  
250 characterization of CePV-TA identified two novel E3L homologs: CePV-TA-20 and CePV-  
251 TA-21 (Rodrigues et al. 2020).

252

253 Our analysis on 11 different E3 homologues revealed that these are highly  
254 divergent: while CPXV 069 (Cowpoxvirus E3 homolog) and TATV 060 (Tateropoxvirus E3  
255 homolog) presented identities of >90% to VACV E3, E3L homologs from poxviruses like  
256 the Deerpoxvirus, Sheeppoxvirus and Yaba monkey poxvirus presented less than 40%  
257 identity (Fig. 5B). Analysis of the two newly identified E3 homologs from CePV-TA shows  
258 that both present low identity to VACV E3, with CePV-TA-20 and CePV-TA-21 proteins

259 only presenting sequence identity of 37 % and 34 %, respectively (Fig. 5B). It is known  
260 that at the amino acid level, the C-terminal of E3-like proteins display a higher level of  
261 sequence similarity than the N-terminal domain (Rahman and McFadden 2020).  
262 Accordingly, the dsRNA-BD domain from CePV-TA-20 and CePV-TA-21 proteins also  
263 display a higher level of sequence similarity compared to other E3 homologs (Fig. 5C),  
264 suggesting that in CeTV this domain might also target conserved antiviral dsRNA-activated  
265 pathways. Similar to what is observed for MPXV and MYXV E3 homologues, both E3  
266 homologs from CePV-TA present incomplete or disrupted N-terminal zNA-BDs. As shown  
267 in Fig. 5C, CePV-TA-20 is missing 20 amino acids in its N-terminal domain. However, this  
268 region still retains the conserved LY and PPXW motifs, as well the basic KKCINR motif  
269 (Fig. 5C), residues known to contact with Z-NA (Kim et al. 2003). Interestingly, MPXV F3  
270 protein, also lacking 37 amino acids from the N-terminal domain, is not able to compete  
271 with ZBP1 and inhibit sensing (unpublished data), even though it retains the key residues  
272 important for binding to Z-NA (Fig. 5C). While CePV-TA-20 and F3 proteins contain an  
273 incomplete zNA-BD, M029 and CePV-TA-21 proteins are missing most of their N-terminal  
274 zNA-BD (Fig. 5B and C), suggesting a total inactivation of this domain and a loss of  
275 function regarding the inhibition of ZBP1-dependent necroptosis. Overall, our results show  
276 that the novel CePV-TA presents two E3L homologues that, like E3L homologues from  
277 MPXV and MYXV, present incomplete or disrupted N-terminal zNA-BD. The presence of  
278 an incomplete or disrupted zNA-BD in E3L homologues highly suggests that these  
279 proteins cannot fully compete with ZBP1 to inhibit necroptosis induction. However, further  
280 studies will be necessary to fully comprehend the action of these proteins regarding  
281 complete necroptosis inhibition.

## 282 Discussion

283 Necroptosis is an inflammatory form of cell death that is mediated by RIPK3 and  
284 MLKL and provides an extra defense mechanism against pathogen infection, facilitating  
285 the elimination of virus-infected cells before the production of progeny virions (Upton and  
286 Chan 2014; Nogusa et al. 2016; Xia et al. 2020). Given the crucial role of necroptosis in  
287 the innate immune response of humans and mice (Orzalli and Kagan 2017; Nailwal and  
288 Chan 2019), it was broadly accepted that this pathway was ubiquitous in mammals. Our  
289 results from 67 species across nine mammalian lineages provides the first comprehensive  
290 picture of the molecular evolution of necroptosis in mammals. We show that while RIPK1  
291 is under evolutionary conservation, RIPK3 and MLKL are poorly conserved in lineages that  
292 evolved separately over the course of evolution.

293

294 A detailed analysis of RIPK3 and MLKL in mammals reveals a complex pattern  
295 where lagomorphs, cetaceans, carnivores and species from rodent and afrotheria lineages  
296 separately lost key components of the necroptotic pathway (Fig. 2A). The order  
297 lagomorpha includes two big families, Ochotonidae and Leporidae (Melo-Ferreira et al.  
298 2015). The presence of the same frameshift mutation in Leporid species (+G, Fig. 3A)  
299 suggests that the disruption of the necroptotic pathway occurred early, but only after the  
300 bifurcation between Ochotona and Leporid given that the plateau Pika presents intact  
301 RIPK3 and MLKL proteins (Fig. 2A). Despite all efforts, and despite the complete genome  
302 assembly surrounding the MLKL flanking genes in the European rabbit genome, no partial  
303 or complete MLKL gene was found, indicating that this gene is deleted in the European  
304 rabbit genome and possibly in the remaining Leporid species (Fig. 4). The core genes of  
305 the necroptotic pathway also presented premature stop codons in cetaceans. In the  
306 studied cetaceans, the MLKL gene presented a common stop codon in the first exon,  
307 resulting in the inactivation of this gene (Fig. 3B). Again, the presence of similar patterns of  
308 pseudogenization in RIPK3 or MLKL genes within species of the same order infer that  
309 disruption of these genes occurred before their diversification and was maintained  
310 throughout evolution. On the other hand, *RIPK3* disruption in cetaceans appears to be the  
311 result of insertions or deletions that are not shared between closely related species, but  
312 rather specific to each species (S Appendix 6), suggesting that these disrupting mutations  
313 occurred later in evolution when compared to MLKL. The addition of some rodents as well  
314 as afrotheria species to the list of mammals that have disrupted necroptotic pathways,  
315 raises the possibility that other closely related species might have lost this pathway after

316 the diversification of these lineages. It is currently believed that activation of the RIPK3 and  
317 recruitment of MLKL are critical steps during necroptosis. For example, deleting either  
318 RIPK3 or MLKL can lead to the suppression of skin and liver inflammation in mice  
319 (Dannappel et al. 2014; Rickard et al. 2014). Moreover, when mice are treated  
320 intravenously with a high-doses of TNF, there appears to be no differences between  
321 RIPK3-deficient and MLKL-deficient mice (Moerke et al. 2019), substantiating the premise  
322 that MLKL follows RIPK3 in the necroptotic signalling. However, this appears not to be the  
323 case for all necroptotic cell death responses, as different studies revealed alternative  
324 pathways for MLKL and RIPK3-dependent programmed necrosis that are executed in the  
325 absence of RIPK3 or MLKL, respectively (Günther et al. 2016; Zhang et al. 2016). To date,  
326 there are no studies suggesting that RIPK3/MLKL double-knockout mice are still able to  
327 induce necroptosis, which indicates that species that have disrupted RIPK3 and MLKL lost  
328 the necroptotic pathway throughout evolution.

329

330 The loss of function of *RIPK3* and *MLKL* in independently evolving lineages  
331 (convergent evolution) indicates that gene loss is an important evolutionary mechanism for  
332 phenotypic change in these animals and may contribute to similar adaptations. Even  
333 though it would be expected that loss of genes is maladaptive, gene loss can be beneficial  
334 by providing an evolutionary mechanism for adaptations. In fact, if the loss of an existing  
335 gene would increase fitness by making a species better adapted to the environment that  
336 surrounds it, then gene loss would be an easy solution to an evolutionary problem.  
337 Necroptosis contributes to innate immunity as a pathogen clearance mechanism (Xia et al.  
338 2020). However, contrary to apoptosis, in which several highly immunogenic intracellular  
339 proteins are sequestered in the dead cell, necroptosis releases DAMPs in the surrounding  
340 tissue that promote strong inflammatory responses and result in the attraction of different  
341 types of immune cells to the site of infection (Kaczmarek et al. 2013). Studies in mouse  
342 models have provided strong evidence that necroptosis is implicated in several  
343 inflammatory neurodegenerative diseases, including multiple sclerosis and amyotrophic  
344 lateral sclerosis (Ofengeim et al. 2015; Ito et al. 2016). Mouse-model experiments  
345 identified keratinocyte necroptosis as a trigger of skin inflammation (Bonnet et al. 2011)  
346 and a correlation between necroptosis and intestinal inflammation has also been  
347 established (Welz et al. 2011; Pierdomenico et al. 2014). Thus, while necroptosis might  
348 mediate host defense, its inhibition in certain contexts may lessen disease severity. It is  
349 known that excessive inflammation can promote cancer cell growth and metastasis

350 (Najafov et al. 2017). Thus, it is possible that a pro-inflammatory cell death like necroptosis  
351 might promote metastasis and thus, inhibition of this pathway might represent an  
352 advantage for regulation of cancer cell growth. Intriguingly, some of the species that are  
353 lacking the core necroptotic machinery are known to resist cancer. That is the case for  
354 cetaceans, the naked mole-rat and african elephants (Liang et al. 2010; Abegglen et al.  
355 2015; Tejada-Martinez et al. 2021). It is also possible that selection against necroptosis in  
356 different mammalian lineages could have been driven by different factors depending on  
357 the environment or conditions. For example, it was previously suggested that the absence  
358 of MLKL in Carnivores reflected a microbe-rich and virus-containing diet of raw meat,  
359 causing evolutionary counter-selection against necroptosis (Dondelinger et al. 2016).  
360 Nevertheless, the absence of the necroptotic pathway in independently evolving lineages  
361 suggest that the deregulation of this pathway was detrimental for the host organism, which  
362 ultimately drove selection against the presence of RIPK3 and MLKL.

363

364 As many other viruses, poxviruses express immunomodulatory and host-range  
365 factors important for the suppression and evasion of the host innate and adaptive antiviral  
366 responses (Werden et al. 2008; Oliveira et al. 2017). VACV protein E3 not only sequester  
367 dsRNA through their dsRNA-BD limiting the activation of the innate immune system  
368 against the virus infection, but also inhibit the IFN-induced dsRNA dependent protein  
369 kinase (PKR), known to be a crucial component of the host innate immunity against viral  
370 infection, replication, and spread (Davies et al. 1993; Sharp et al. 1998). Our results show  
371 that the dsRNA-BD of distant E3L proteins present high levels of sequence similarity (Fig.  
372 5B and C), which is consistent with the ability of this domain to target conserved pathways  
373 present in different hosts. Although the dsRNA sequestration functions of the E3 C-  
374 terminal have been clear for decades (Chang and Jacobs 1993; Thompson et al. 1994),  
375 the IFN sensitivity of VACV E3 N-terminal deletion mutants remained unresolved for a long  
376 time. Recently, strong evidence showed that the E3 N-terminal domain competes with  
377 ZBP1 to prevent ZBP1-dependent activation of RIPK3 and consequent necroptosis  
378 (Koehler et al. 2017; Koehler et al. 2020). The model proposed by the authors suggests  
379 that during WT-VACV infection, the zNA-BD of E3 binds to VACV-induced Z-form nucleic  
380 acid and masks it, preventing sensing by ZBP1 and further RIPK3 necroptosis induction  
381 (Koehler et al. 2017; Koehler et al. 2020). However, it is interesting that poxviruses like  
382 MPXV, MYXV and CePV-TA have E3L homologs that present a complete dsRNA-BD but  
383 not zNA-BD (Fig. 5B). In VACV-E3  $\Delta$ 83N-infected cells (mutant lacking the first 83 aa

384 corresponding to the zNA-BD), the absence of the zNA-BD facilitates ZBP1 to sense  
385 VACV-induced PAMPs and initiate necroptosis induction (Koehler et al. 2017). Therefore,  
386 it is expected that E3L homologues that lack N-terminal zNA domains, like CePV-TA-21  
387 and M029, cannot prevent Z-form nucleic acid sensing triggering necroptosis induction and  
388 early abortion of viral replication. Like CePV-TA-20, F3 protein is also missing several  
389 amino acids in the N-terminal region and presents high conservation in areas that are  
390 known to bind to zNA (Fig. 5C). Nevertheless, F3 protein seems to have lost the ability to  
391 compete with ZBP1 and inhibit sensing (unpublished data). It was previously shown that  
392 the N-terminus of VACV E3 is necessary for IFN resistance in JC cells since VACV-  
393 E3 $\Delta$ 37N (mutant mimicking MPXV E3 zNA-BD) did not initiate DNA replication (Arndt et al.  
394 2015). However, MPXV was able to replicate efficiently in the same cells, despite having a  
395 partial N-terminal zNA-BD, suggesting that the predicted binding to z-form nucleic acid  
396 was intragenic and downstream of z-NA sensing, rather than related to the ability of F3  
397 zNA-BD to mask z-form nucleic acid (Arndt et al. 2015).

398

399 Interestingly, inactivation of necroptosis in Lagomorphs and Cetaceans seems to  
400 correlate with the absence of the E3L zNA-BD in their naturally infecting poxviruses,  
401 namely leporipoxviruses (MYXV and SFV) and cetaceanpoxviruses (CePV-TA),  
402 respectively. Monkeypox is a viral zoonosis endemic to central and western Africa areas  
403 where African rope squirrels and other rodents are likely reservoir hosts (Essbauer et al.  
404 2010). Interestingly, the absence of a functional N-terminus in MPXV F3 protein also  
405 seems to correlate with the fact that some rodents appear incapable of undergoing  
406 necroptosis. Like MPXV, leporipoxviruses and CePV-TA pathogenesis are restricted to  
407 only certain species and have little or no pathogenesis capability in all others (Rahman et  
408 al. 2013; Arndt et al. 2015; Rodrigues et al. 2020). Infection of the same host over  
409 hundreds of years or even millennia may drive the evolution of each virus to rapidly evolve  
410 to a fitness peak in a given host environment. Previous niche-filling models (Holt 2009;  
411 Cooper et al. 2010; Simmonds et al. 2019) emphasize the role of host interactions in  
412 shaping virus evolution. According to these models, as hosts diversify and speciate over  
413 longer evolutionary periods, viral host factors that aim to counter the host antiviral  
414 functions are subject to continuous changes. Indeed, it is known that genes associated  
415 with host antiviral mechanisms present high evolutionary rates and are often under  
416 positive selection (Münk et al. 2012; van der Lee et al. 2017; Águeda-Pinto, Lemos de  
417 Matos, et al. 2019). Here, we suggest that during the evolution of these poxviruses, the

418 loss of the zNA-BD did not present a disadvantage in the host organism; therefore, this  
419 trait was maintained, which reflects how these viruses adapt as their niche changed.

420

## 421 **Concluding remarks**

422 The disruption of necroptosis in independently evolving lineages suggests a  
423 convergent evolutionary loss of this pathway, probably reflecting an important selective  
424 mechanism for phenotypic change. Interestingly, we also found a strong correlation  
425 between the disruption of necroptosis in leporids and cetaceans and the absence of the  
426 E3L zNA-BD (responsible for necroptosis inhibition) in their naturally infecting poxviruses  
427 as in the case of MYXV and CePV-TA, respectively. Overall, our study provides the first  
428 comprehensive picture of the molecular evolution of necroptosis in mammals, highlighting  
429 the importance of gene/pathway loss for the process of species adaptation and suggesting  
430 that it is a true pathogen-response pathway that is not required for normal mammalian  
431 development. Moreover, this study sheds some light on a co-evolutionary relationship  
432 between poxviruses and their hosts, emphasizing the role of host adaptation in shaping  
433 virus evolution.

## 434 **Materials and Methods**

### 435 **Genomic approach to detect genes associated with the necroptosis pathway**

436 To detect intact and inactivated genes, we first identified the key genes of the  
437 necroptotic pathway (i.e., *RIPK1*, *RIPK3* and *MLKL*) in the human (*H. sapiens*) and mouse  
438 (*Mus musculus*) reference genomes and looked for the presence of orthologues in existing  
439 genome sequence databases from 67 different species that belong to the 9 main  
440 mammalian orders/superorders: primates, rodents, lagomorpha, chiroptera, carnivora,  
441 perissodactyla, artiodactyla, cetacea, and afrotheria (S Appendix 1). We did not only  
442 search for the complete loss of exons or entire genes, but also searched for insertions and  
443 deletions that shift the reading frame, frame-preserving insertions that create a premature  
444 stop codon and substitutions that create an in-frame stop codon. The respective search  
445 methodology had been previously applied to the identification of different homologues of  
446 different annotated mammalian genomes (Sharma et al. 2018; Águeda-Pinto, Castro, et al.  
447 2019). To further ensure that all gene loss events discussed in this study are real and not  
448 due to sequencing errors, we validated them either by sequencing of samples or by using  
449 a curated bioinformatic pipeline (see below).

450

### 451 **Amplification and sequencing of *RIPK1* and *RIPK3* nucleic acid sequences from** 452 **Lagomorpha species**

453 In contrast to the majority of mammalian orders, lagomorpha only presents three  
454 annotated genomes: the European rabbit (*Oryctolagus cuniculus*, accession #  
455 GCA\_000003625.1), the American Pika genome (*Ochotona princeps*, accession #  
456 GCA\_014633375.1) and the plateau pika (*O. curzoniae*, accession # GCA\_017591425.1).  
457 Given the importance of lagomorphs for this study, samples from different lagomorpha  
458 species were used to obtain the nucleic coding sequence from *RIPK1*. For that, RNA was  
459 extracted from tissues of *O. cuniculus cuniculus*, *O. cuniculus algirus*, *Lepus americanus*,  
460 *L. europaeus*, *L. timidus*, *L. granatensis*, *Sylvilagus floridanus*, *S. bachmanis*, *O. princeps*  
461 and *O. collaris* samples, using the Qiagen DNeasy Blood & Tissue kit (Qiagen, USA)  
462 following manufacturer's instructions. Synthesis of cDNA was achieved by using  
463 SuperScript III Reverse Transcriptase (Invitrogen, USA). Primers were designed according  
464 to the *RIPK1* transcript from *O. cuniculus* [Accession # XM\_017350509.1] (Forward 5'-  
465 ATGTCTTTGGATGACATTTAAATG-3' and Reverse 5'-CTACTTCTGGCTGAGCTGTATC-  
466 3') and used to amplify the samples mentioned before. Phusion<sup>®</sup> High-Fidelity DNA  
467 Polymerase (Finnzymes, Espoo, Finland) was used in the PCR amplification and the



468 conditions included an initial denaturation (98°C for 3min), 35 cycles of denaturation (98°C  
469 for 30s), annealing (60°C for 15s) and extension (72°C for 30s) followed a final extension  
470 (72°C for 5 min).

471

472 From our initial search, the *RIPK3* gene was not annotated in the European rabbit.  
473 However, after mapping the location of *RIPK3* based on its location in *H. sapiens*, *M.*  
474 *musculus* and *O. curzoniae*, we were able to identify a partial *RIPK3* sequence in the  
475 European rabbit genome that presented an early stop codon. To exclude potential artifacts  
476 that can mimic real gene-inactivating mutations, a forward (5'-  
477 ATGTCTTCTGTCAAATTGTGG-3') and a reverse (5'-ACTGCCTGCATCAGGATC-3')  
478 primer were designed based on the parcial *RIPK3* sequence and were used to amplify the  
479 same region in the genomes from *O. cuniculus cuniculus*, *S. floridanus*, *L. americanus*, *L.*  
480 *europaeus* and *L. saxatilis*. For that, genomic DNA was extracted using the Qiagen  
481 DNeasy Blood & Tissue kit (Qiagen, USA) according to the manufacturer's instructions.  
482 Phusion® High-Fidelity DNA Polymerase (Finnzymes, Espoo, Finland) was used in the  
483 PCR amplification and the conditions included an initial denaturation (98°C for 3min), 9  
484 cycles of denaturation (98°C for 30s), annealing (66°C for 15s) and extension (72°C for  
485 30s) followed by more 25 cycles of denaturation (98°C for 30s), annealing (61°C for 15s)  
486 and extension (72°C for 30s) and a final extension (72°C for 5min).

487

488 Amplicons sequencing from *RIPK1* and *RIPK3* was performed with the ABI PRISM  
489 BigDye Terminator v3.1 Cycle Sequencing Kit and according to manufacturer's protocol;  
490 reactions were cleaned with Sephadex™ (GE Healthcare Life Sciences, UK) and applied  
491 on an ABI PRISM 310 Genetic Analyser (Life Technologies, Applied Biosystems,  
492 Carlsbad, CA, USA). The obtained *RIPK1* coding sequences and the partial *RIPK3*  
493 sequences from the different Lagomorphs have been deposited in the GenBank database  
494 under the accession numbers that are shown in S Appendix 2. All samples were supplied  
495 by CIBIO/InBIO, Vairão, Portugal and used in previous studies (de Matos et al. 2011;  
496 Águeda-Pinto, Lemos de Matos, et al. 2019). No animals were captured, handled, or killed  
497 specifically for the purpose of this study.

498

#### 499 **Detailed analysis on the cetacean genomes**

500 Briefly, NCBI gene annotations for the gene orthologues of *MLKL* and *RIPK3* were  
501 initially screened via PseudoChecker ([pseudochecker.ciimar.up.pt](http://pseudochecker.ciimar.up.pt)), which evaluates the

502 coding condition of a gene (Ranwez et al. 2018; Alves et al. 2020). For each gene, a  
503 PseudoChecker analysis was run (default parameters), using the *Bos taurus* (cow) gene  
504 orthologue as a comparative input (NCBI Accession ID regarding cow MLKL:  
505 XM\_002694707.6; RIPK3: XM\_024997365.1), as well as the genomic sequences  
506 encompassing the putative ORF of the orthologous counterpart of each target species,  
507 directly exported from the NCBI genome browser. Through PseudoIndex, a built-in  
508 assistant metric, we quickly assessed the erosion status of the tested genes on a discrete  
509 scale ranging from 0 (coding) to 5 (pseudogenized) (Alves et al. 2020). Subsequent  
510 manual annotation was performed by importing the previously collected genomic  
511 sequences into Geneious Prime 2020 software ([www.geneious.com](http://www.geneious.com)) (Kearse et al. 2012)  
512 and determining each gene's CDS using as reference cow's *MLKL* and *RIPK3* orthologues  
513 sequences. In detail, per gene and species, using the built-in map to reference tool  
514 (highest sensitivity parameter selected), each (3' and 5' untranslated region-flanked)  
515 reference coding-exon was mapped against each target genomic sequence. Exons  
516 alignments were further screened for gene disruptive mutations, including in-frame  
517 premature stop codons, frameshift, and splice site mutations (any deviation from the  
518 consensus donor splice site GT/GC or the consensus acceptor splice site AG).

519

520 To inspect if the identified genetic lesions were not rendered as result of  
521 sequencing and/or genome assembly artifacts, we performed mutational validation (one  
522 per gene and species), resorting of raw genomic sequencing reads, retrieved from two  
523 independent genomic projects from the NCBI sequence read archive (SRA), when  
524 available. Explicitly, blastn searches were directed to the selected SRA projects, using the  
525 nucleotide sequence portion containing the selected mutation(s) as a query. The matching  
526 sequencing reads were downloaded into Geneious Prime 2020 (Kearse et al. 2012)  
527 software and mapped against the manually annotated mutation (highest sensibility  
528 parameter selected), confirming, or not, the presence of the identified mutation.

529

### 530 **Phylogenetic and molecular evolutionary analyses**

531 The complete dataset of RIPK1, RIPK3 and MLKL proteins was aligned in BioEdit  
532 Sequence Alignment Editor using Clustal W (Thompson et al. 1994), followed by manual  
533 corrections when necessary. Amino acid alignments were then used to infer Maximum  
534 Likelihood (ML) phylogenetic trees using MEGA X (Kumar et al. 2018), with the

535 substitution models JTT+G+F, JTT+G and HKY+G+I, respectively; determined using  
536 ProtTest (Darriba et al. 2011).

537

538         Given the fact that RIPK3 and MLKL proteins are highly divergent across the  
539 studied mammalian species, we decided not to perform any evolutionary analysis using  
540 these alignments. To look for signatures of natural selection operating in the RIPK1  
541 alignment, we used HyPhy software implemented in the Datamonkey Web server (Pond  
542 and Frost 2005), to detect codons under selection: the Single Likelihood Ancestor  
543 Counting (SLAC) model, the Fixed Effect Likelihood (FEL) method (Kosakovsky Pond and  
544 Frost 2005), the Random Effect Likelihood, the Mixed Effects Model of Evolution (MEME)  
545 (Murrell et al. 2012) and Fast Unbiased Bayesian AppRoximation (FUBAR) (Murrell et al.  
546 2013) methods were used. To avoid a high false positive rate, codons with p-values <0.05  
547 for SLAC, FEL and MEME models and a posterior probability >0.95 for FUBAR were  
548 accepted as candidates for selection. For a more conservative approach, only residues  
549 identified as being under positive selection in three or more ML methods were considered.

550

#### 551 **Analysis of VACV E3 homologues**

552         VACV E3 homologues encoded by different poxviruses (=11) were retrieved from  
553 the NCBI database (<https://www.ncbi.nlm.nih.gov/>) and aligned in the BioEdit Sequence  
554 Alignment Editor using Clustal W (Thompson et al. 1994), followed by manual corrections  
555 when necessary. Amino acid alignments of the representative E3-like proteins were used  
556 to generate schematic diagrams using the COBALT program from the NCBI database.

## 557 **Acknowledgments**

558           This work was supported by Foundation for Science and Technology (FCT), which  
559 supported the doctoral fellowship of A.Á.-P. (ref. SFRH/BD/128752/2017) and the  
560 investigator grant of P.J.E. (IF/00376/2015). This article is also a result of the project  
561 NORTE-01-0145-FEDER-000007, supported by Norte Portugal Regional Operational  
562 Programme (NORTE2020), under the PORTUGAL 2020 Partnership Agreement, through  
563 the European Regional Development Fund (ERDF). GM and MMR's research is supported  
564 by the National Institute of Health (NIH) grants R01AI080607 and R01AI148302.

## 565 References

- 566 Abegglen LM, Caulin AF, Chan A, Lee K, Robinson R, Campbell MS, Kiso WK, Schmitt  
567 DL, Waddell PJ, Bhaskara S, et al. 2015. Potential Mechanisms for Cancer  
568 Resistance in Elephants and Comparative Cellular Response to DNA Damage in  
569 Humans. *JAMA* 314:1850–1860.
- 570 Águeda-Pinto A, Castro LFC, Esteves PJ. 2019. The evolution of S100A7: an unusual  
571 gene expansion in Myotis bats. *BMC Evol. Biol.* 19:102.
- 572 Águeda-Pinto A, Lemos de Matos A, Pinheiro A, Neves F, de Sousa-Pereira P, Esteves  
573 PJ. 2019. Not so unique to Primates: The independent adaptive evolution of TRIM5 in  
574 Lagomorpha lineage. *PLoS One* 14:e0226202.
- 575 Alves LQ, Ruivo R, Fonseca MM, Lopes-Marques M, Ribeiro P, Castro LFC. 2020.  
576 PseudoChecker: an integrated online platform for gene inactivation inference. *Nucleic  
577 Acids Res.* 48:W321–W331.
- 578 Arndt WD, Cotsmire S, Trainor K, Harrington H, Hauns K, Kibler KV, Huynh TP, Jacobs  
579 BL. 2015. Evasion of the Innate Immune Type I Interferon System by Monkeypox  
580 Virus. *J. Virol.* 89:10489–10499.
- 581 Bonnet MC, Preukschat D, Welz P-S, van Loo G, Ermolaeva MA, Bloch W, Haase I,  
582 Pasparakis M. 2011. The adaptor protein FADD protects epidermal keratinocytes from  
583 necroptosis in vivo and prevents skin inflammation. *Immunity* 35:572–582.
- 584 Chang HW, Jacobs BL. 1993. Identification of a conserved motif that is necessary for  
585 binding of the vaccinia virus E3L gene products to double-stranded RNA. *Virology*  
586 194:537–547.
- 587 Cooper N, Jetz W, Freckleton RP. 2010. Phylogenetic comparative approaches for  
588 studying niche conservatism. *J. Evol. Biol.* 23:2529–2539.
- 589 Dannappel M, Vlantis K, Kumari S, Polykratis A, Kim C, Wachsmuth L, Eftychi C, Lin J,  
590 Corona T, Hermance N, et al. 2014. RIPK1 maintains epithelial homeostasis by  
591 inhibiting apoptosis and necroptosis. *Nature* 513:90–94.
- 592 Darriba D, Taboada GL, Doallo R, Posada D. 2011. ProtTest 3: fast selection of best-fit  
593 models of protein evolution. *Bioinformatics* 27:1164–1165.
- 594 Davies MV, Chang HW, Jacobs BL, Kaufman RJ. 1993. The E3L and K3L vaccinia virus  
595 gene products stimulate translation through inhibition of the double-stranded RNA-  
596 dependent protein kinase by different mechanisms. *J. Virol.* 67:1688–1692.
- 597 Dondelinger Y, Hulpiau P, Saeys Y, Bertrand MJM, Vandenabeele P. 2016. An  
598 evolutionary perspective on the necroptotic pathway. *Trends Cell Biol.* 26:721–732.
- 599 Essbauer S, Pfeffer M, Meyer H. 2010. Zoonotic poxviruses. *Vet. Microbiol.* 140:229–236.
- 600 Ge D, Wen Z, Xia L, Zhang Z, Erbajeva M, Huang C, Yang Q. 2013. Evolutionary history  
601 of lagomorphs in response to global environmental change. *PLoS One* 8:e59668.

- 602 Günther C, He G-W, Kremer AE, Murphy JM, Petrie EJ, Amann K, Vandenabeele P,  
603 Linkermann A, Poremba C, Schleicher U, et al. 2016. The pseudokinase MLKL  
604 mediates programmed hepatocellular necrosis independently of RIPK3 during  
605 hepatitis. *J. Clin. Invest.* 126:4346–4360.
- 606 He S, Liang Y, Shao F, Wang X. 2011. Toll-like receptors activate programmed necrosis in  
607 macrophages through a receptor-interacting kinase-3-mediated pathway. *Proc. Natl.*  
608 *Acad. Sci. U. S. A.* 108:20054–20059.
- 609 He S, Wang L, Miao L, Wang T, Du F, Zhao L, Wang X. 2009. Receptor interacting protein  
610 kinase-3 determines cellular necrotic response to TNF-alpha. *Cell* 137:1100–1111.
- 611 He S, Wang X. 2018. RIP kinases as modulators of inflammation and immunity. *Nat.*  
612 *Immunol.* 19:912–922.
- 613 Holt RD. 2009. Bringing the Hutchinsonian niche into the 21st century: ecological and  
614 evolutionary perspectives. *Proc. Natl. Acad. Sci. U. S. A.* 106 Suppl 2:19659–19665.
- 615 Huelsmann M, Hecker N, Springer MS, Gatesy J, Sharma V, Hiller M. 2019. Genes lost  
616 during the transition from land to water in cetaceans highlight genomic changes  
617 associated with aquatic adaptations. *Sci Adv* 5:eaaw6671.
- 618 Ito Y, Ofengeim D, Najafov A, Das S, Saberi S, Li Y, Hitomi J, Zhu H, Chen H, Mayo L, et  
619 al. 2016. RIPK1 mediates axonal degeneration by promoting inflammation and  
620 necroptosis in ALS. *Science* 353:603–608.
- 621 Kaczmarek A, Vandenabeele P, Krysko DV. 2013. Necroptosis: the release of damage-  
622 associated molecular patterns and its physiological relevance. *Immunity* 38:209–223.
- 623 Kaiser WJ, Upton JW, Mocarski ES. 2013. Viral modulation of programmed necrosis. *Curr.*  
624 *Opin. Virol.* 3:296–306.
- 625 Kawasaki K, Mikami M, Goto M, Shindo J, Amano M, Ishiyama M. 2020. The Evolution of  
626 Unusually Small Amelogenin Genes in Cetaceans; Pseudogenization, X-Y Gene  
627 Conversion, and Feeding Strategy. *J. Mol. Evol.* 88:122–135.
- 628 Kearse M, Moir R, Wilson A, Stones-Havas S, Cheung M, Sturrock S, Buxton S, Cooper A,  
629 Markowitz S, Duran C, et al. 2012. Geneious Basic: an integrated and extendable  
630 desktop software platform for the organization and analysis of sequence data.  
631 *Bioinformatics* 28:1647–1649.
- 632 Kim Y-G, Lowenhaupt K, Oh D-B, Kim KK, Rich A. 2004. Evidence that vaccinia virulence  
633 factor E3L binds to Z-DNA in vivo: Implications for development of a therapy for  
634 poxvirus infection. *Proc. Natl. Acad. Sci. U. S. A.* 101:1514–1518.
- 635 Kim Y-G, Muralinath M, Brandt T, Pearcy M, Hauns K, Lowenhaupt K, Jacobs BL, Rich A.  
636 2003. A role for Z-DNA binding in vaccinia virus pathogenesis. *Proc. Natl. Acad. Sci.*  
637 *U. S. A.* 100:6974–6979.
- 638 Koehler H, Cotsmire S, Langland J, Kibler KV, Kalman D, Upton JW, Mocarski ES, Jacobs  
639 BL. 2017. Inhibition of DAI-dependent necroptosis by the Z-DNA binding domain of  
640 the vaccinia virus innate immune evasion protein, E3. *Proc. Natl. Acad. Sci. U. S. A.*

- 641 114:11506–11511.
- 642 Koehler HS, Cotsmire S, Zhang T, Balachandran S, Upton JW, Langland J, Kalman D,  
643 Jacobs BL, Mocarski ES. 2020. Competition between E3 and ZBP1 for Z-RNA  
644 dictates susceptibility to Vaccinia virus-induced necroptosis. *SSRN Electron. J.*  
645 [Internet]. Available from: <https://www.ssrn.com/abstract=3717768>
- 646 Kosakovsky Pond SL, Frost SDW. 2005. Not so different after all: a comparison of  
647 methods for detecting amino acid sites under selection. *Mol. Biol. Evol.* 22:1208–  
648 1222.
- 649 Kosiol C, Vinar T, da Fonseca RR, Hubisz MJ, Bustamante CD, Nielsen R, Siepel A. 2008.  
650 Patterns of positive selection in six Mammalian genomes. *PLoS Genet.* 4:e1000144.
- 651 Kumar S, Stecher G, Li M, Knyaz C, Tamura K. 2018. MEGA X: Molecular Evolutionary  
652 Genetics Analysis across Computing Platforms. *Mol. Biol. Evol.* 35:1547–1549.
- 653 van der Lee R, Wiel L, van Dam TJP, Huynen MA. 2017. Genome-scale detection of  
654 positive selection in nine primates predicts human-virus evolutionary conflicts. *Nucleic  
655 Acids Res.* 45:10634–10648.
- 656 Liang S, Mele J, Wu Y, Buffenstein R, Hornsby PJ. 2010. Resistance to experimental  
657 tumorigenesis in cells of a long-lived mammal, the naked mole-rat (*Heterocephalus  
658 glaber*). *Aging Cell* 9:626–635.
- 659 Li J, McQuade T, Siemer AB, Napetschnig J, Moriwaki K, Hsiao Y-S, Damko E, Moquin D,  
660 Walz T, McDermott A, et al. 2012. The RIP1/RIP3 necrosome forms a functional  
661 amyloid signaling complex required for programmed necrosis. *Cell* 150:339–350.
- 662 de Matos AL, van der Loo W, Areal H, Lanning DK, Esteves PJ. 2011. Study of *Sylvilagus*  
663 rabbit TRIM5 $\alpha$  species-specific domain: how ancient endoviruses could have shaped  
664 the antiviral repertoire in Lagomorpha. *BMC Evol. Biol.* 11:294.
- 665 McGowen MR, Tsagkogeorga G, Álvarez-Carretero S, Dos Reis M, Struebig M, Deaville  
666 R, Jepson PD, Jarman S, Polanowski A, Morin PA, et al. 2020. Phylogenomic  
667 Resolution of the Cetacean Tree of Life Using Target Sequence Capture. *Syst. Biol.*  
668 69:479–501.
- 669 Melo-Ferreira J, Lemos de Matos A, Areal H, Lissovsky AA, Carneiro M, Esteves PJ.  
670 2015. The phylogeny of pikas (*Ochotona*) inferred from a multilocus coalescent  
671 approach. *Mol. Phylogenet. Evol.* 84:240–244.
- 672 Meng H, Liu Z, Li X, Wang H, Jin T, Wu G, Shan B, Christofferson DE, Qi C, Yu Q, et al.  
673 2018. Death-domain dimerization-mediated activation of RIPK1 controls necroptosis  
674 and RIPK1-dependent apoptosis. *Proc. Natl. Acad. Sci. U. S. A.* 115:E2001–E2009.
- 675 Mifflin L, Ofengeim D, Yuan J. 2020. Receptor-interacting protein kinase 1 (RIPK1) as a  
676 therapeutic target. *Nat. Rev. Drug Discov.* 19:553–571.
- 677 Moerke C, Bleibaum F, Kunzendorf U, Krautwald S. 2019. Combined Knockout of RIPK3  
678 and MLKL Reveals Unexpected Outcome in Tissue Injury and Inflammation. *Front  
679 Cell Dev Biol* 7:19.

- 680 Münk C, Willemsen A, Bravo IG. 2012. An ancient history of gene duplications, fusions  
681 and losses in the evolution of APOBEC3 mutators in mammals. *BMC Evol. Biol.*  
682 12:71.
- 683 Murrell B, Moola S, Mabona A, Weighill T, Sheward D, Kosakovsky Pond SL, Scheffler K.  
684 2013. FUBAR: a fast, unconstrained bayesian approximation for inferring selection.  
685 *Mol. Biol. Evol.* 30:1196–1205.
- 686 Murrell B, Wertheim JO, Moola S, Weighill T, Scheffler K, Kosakovsky Pond SL. 2012.  
687 Detecting individual sites subject to episodic diversifying selection. *PLoS Genet.*  
688 8:e1002764.
- 689 Nailwal H, Chan FK-M. 2019. Necroptosis in anti-viral inflammation. *Cell Death Differ.*  
690 26:4–13.
- 691 Najafov A, Chen H, Yuan J. 2017. Necroptosis and Cancer. *Trends Cancer Res.* 3:294–  
692 301.
- 693 Nogusa S, Thapa RJ, Dillon CP, Liedmann S, Oguin TH 3rd, Ingram JP, Rodriguez DA,  
694 Kosoff R, Sharma S, Sturm O, et al. 2016. RIPK3 Activates Parallel Pathways of  
695 MLKL-Driven Necroptosis and FADD-Mediated Apoptosis to Protect against Influenza  
696 A Virus. *Cell Host Microbe* 20:13–24.
- 697 Ofengeim D, Ito Y, Najafov A, Zhang Y, Shan B, DeWitt JP, Ye J, Zhang X, Chang A,  
698 Vakifahmetoglu-Norberg H, et al. 2015. Activation of necroptosis in multiple sclerosis.  
699 *Cell Rep.* 10:1836–1849.
- 700 Oliveira GP, Rodrigues RAL, Lima MT, Drumond BP, Abrahão JS. 2017. Poxvirus Host  
701 Range Genes and Virus-Host Spectrum: A Critical Review. *Viruses* [Internet] 9.  
702 Available from: <http://dx.doi.org/10.3390/v9110331>
- 703 Orzalli MH, Kagan JC. 2017. Apoptosis and Necroptosis as Host Defense Strategies to  
704 Prevent Viral Infection. *Trends Cell Biol.* 27:800–809.
- 705 Pierdomenico M, Negroni A, Stronati L, Vitali R, Prete E, Bertin J, Gough PJ, Aloï M,  
706 Cucchiara S. 2014. Necroptosis is active in children with inflammatory bowel disease  
707 and contributes to heighten intestinal inflammation. *Am. J. Gastroenterol.* 109:279–  
708 287.
- 709 Pond SLK, Frost SDW. 2005. Datamonkey: rapid detection of selective pressure on  
710 individual sites of codon alignments. *Bioinformatics* 21:2531–2533.
- 711 Rahman MM, Liu J, Chan WM, Rothenburg S, McFadden G. 2013. Myxoma virus protein  
712 M029 is a dual function immunomodulator that inhibits PKR and also conscripts  
713 RHA/DHX9 to promote expanded host tropism and viral replication. *PLoS Pathog.*  
714 9:e1003465.
- 715 Rahman MM, McFadden G. 2020. Myxoma Virus-Encoded Host Range Protein M029: A  
716 Multifunctional Antagonist Targeting Multiple Host Antiviral and Innate Immune  
717 Pathways. *Vaccines (Basel)* [Internet] 8. Available from:  
718 <http://dx.doi.org/10.3390/vaccines8020244>



- 719 Ranwez V, Douzery EJP, Cambon C, Chantret N, Delsuc F. 2018. MACSE v2: Toolkit for  
720 the Alignment of Coding Sequences Accounting for Frameshifts and Stop Codons.  
721 *Mol. Biol. Evol.* 35:2582–2584.
- 722 Rickard JA, Anderton H, Etemadi N, Nachbur U, Darding M, Peltzer N, Lalaoui N, Lawlor  
723 KE, Vanyai H, Hall C, et al. 2014. TNFR1-dependent cell death drives inflammation in  
724 Sharpin-deficient mice. *Elife* [Internet] 3. Available from:  
725 <http://dx.doi.org/10.7554/eLife.03464>
- 726 Rodrigues TCS, Subramaniam K, Varsani A, McFadden G, Schaefer AM, Bossart GD,  
727 Romero CH, Waltzek TB. 2020. Genome characterization of cetaceanpox virus from a  
728 managed Indo-Pacific bottlenose dolphin (*Tursiops aduncus*). *Virus Res.* 278:197861.
- 729 Sharma V, Hecker N, Roscito JG, Foerster L, Langer BE, Hiller M. 2018. A genomics  
730 approach reveals insights into the importance of gene losses for mammalian  
731 adaptations. *Nat. Commun.* 9:1215.
- 732 Sharp TV, Moonan F, Romashko A, Joshi B, Barber GN, Jagus R. 1998. The vaccinia  
733 virus E3L gene product interacts with both the regulatory and the substrate binding  
734 regions of PKR: implications for PKR autoregulation. *Virology* 250:302–315.
- 735 Simmonds P, Aiewsakun P, Katzourakis A. 2019. Prisoners of war - host adaptation and  
736 its constraints on virus evolution. *Nat. Rev. Microbiol.* 17:321–328.
- 737 Sun L, Wang H, Wang Z, He S, Chen S, Liao D, Wang L, Yan J, Liu W, Lei X, et al. 2012.  
738 Mixed lineage kinase domain-like protein mediates necrosis signaling downstream of  
739 RIP3 kinase. *Cell* 148:213–227.
- 740 Sun X, Yin J, Starovasnik MA, Fairbrother WJ, Dixit VM. 2002. Identification of a novel  
741 homotypic interaction motif required for the phosphorylation of receptor-interacting  
742 protein (RIP) by RIP3. *J. Biol. Chem.* 277:9505–9511.
- 743 Tejada-Martinez D, de Magalhães JP, Opazo JC. 2021. Positive selection and gene  
744 duplications in tumour suppressor genes reveal clues about how cetaceans resist  
745 cancer. *Proc. Biol. Sci.* 288:20202592.
- 746 Thompson JD, Higgins DG, Gibson TJ. 1994. CLUSTAL W: improving the sensitivity of  
747 progressive multiple sequence alignment through sequence weighting, position-  
748 specific gap penalties and weight matrix choice. *Nucleic Acids Res.* 22:4673–4680.
- 749 Upton JW, Chan FK-M. 2014. Staying alive: cell death in antiviral immunity. *Mol. Cell*  
750 54:273–280.
- 751 Upton JW, Kaiser WJ, Mocarski ES. 2010. Virus inhibition of RIP3-dependent necrosis.  
752 *Cell Host Microbe* 7:302–313.
- 753 Upton JW, Kaiser WJ, Mocarski ES. 2012. DAI/ZBP1/DLM-1 complexes with RIP3 to  
754 mediate virus-induced programmed necrosis that is targeted by murine  
755 cytomegalovirus vIRA. *Cell Host Microbe* 11:290–297.
- 756 Welz P-S, Wullaert A, Vlantis K, Kondylis V, Fernández-Majada V, Ermolaeva M, Kirsch P,  
757 Sterner-Kock A, van Loo G, Pasparakis M. 2011. FADD prevents RIP3-mediated

- 758 epithelial cell necrosis and chronic intestinal inflammation. *Nature* 477:330–334.
- 759 Werden SJ, Rahman MM, McFadden G. 2008. Poxvirus host range genes. *Adv. Virus*  
760 *Res.* 71:135–171.
- 761 Xia X, Lei L, Wang S, Hu J, Zhang G. 2020. Necroptosis and its role in infectious diseases.  
762 *Apoptosis* 25:169–178.
- 763 Zhang D-W, Shao J, Lin J, Zhang N, Lu B-J, Lin S-C, Dong M-Q, Han J. 2009. RIP3, an  
764 energy metabolism regulator that switches TNF-induced cell death from apoptosis to  
765 necrosis. *Science* 325:332–336.
- 766 Zhang T, Zhang Y, Cui M, Jin L, Wang Y, Lv F, Liu Y, Zheng W, Shang H, Zhang J, et al.  
767 2016. CaMKII is a RIP3 substrate mediating ischemia- and oxidative stress-induced  
768 myocardial necroptosis. *Nat. Med.* 22:175–182.

769 **Figure captions**

770 **Fig. 1 The necroptosis signaling pathway.** Simplified schematic representation of the  
771 necroptosis signaling pathway upon stimulation of the TNFR, TRF3/4 and infection by  
772 poxviruses. All of these necroptosis-inducing signals converge on the kinase RIPK3, which  
773 is activated through the homotypic interaction with RIPK1 or other RHIM-containing  
774 proteins, such as TRIF and DAI. When the activity of caspase-8 is inhibited, binding of  
775 TNF to TNFR1 leads to the phosphorylation and activation of RIPK1 that binds to RIPK3  
776 through their RHIM domains to form a protein complex (necrosome). Activated RIPK3  
777 recruits MLKL that oligomerizes and translocates to the plasma membrane to cause  
778 necroptosis. In TLR3- and TLR4-induced necroptosis, TRIF is required for the activation of  
779 RIPK3. ZBP1 is required for the activation of RIPK3 in response to the presence of Z-form  
780 nucleic acids. In VACV-infected cells, the poxviral E3 protein binds to VACV-induced Z-  
781 form nucleic acid, preventing RIPK3-induced necroptosis. Abbreviations: TNFR, tumor  
782 necrosis factor receptor; TLR 3/4, toll-like receptor; TRIF, TIR-domain-containing adaptor-  
783 inducing IFN  $\beta$ ; RIP, receptor-interacting protein kinase; ZBP1, Z-DNA binding protein;  
784 MLKL, mixed-lineage kinase domain like.

785 **Fig. 2 Evolution of RIPK1, RIPK3 and MLKL in different mammalian lineages. A)**  
786 Phylogenetic tree showing the independent lineages that lost necroptotic core proteins  
787 (RIPK3 and MLKL) during evolution. Green circles represent genes that are present in the  
788 studied species, red circles represent genes that are disrupted, yellow circles represent  
789 genes that have incomplete assemblies and grey rectangles indicate that genes were not  
790 found in those species genomes. **B)** A schematic diagram of RIPK1, RIPK3 and MLKL  
791 domains. RIPK1 contains an N-terminal kinase domain (KD), an intermediate domain with  
792 a RIP homotypic interaction motif (RHIM), and a C-terminal death domain (DD). The  
793 phosphorylation and ubiquitination sites are indicated above the RIPK1 domains. Red  
794 circles represent residues that are under positive selection. RIPK3 contains a KD and a  
795 RHIM domain. MLKL is composed of an N-terminal bundle four-helix bundle (4HD) domain  
796 that is regulated by the C-terminal pseudokinase domain (PKD).

797 **Fig. 3 Loss of *RIPK3* and *MLKL* genes in the steam lineage of Leporids and**  
798 **Cetaceans. A)** Genomic analysis of the first tree exons from Leporids (marked as dark  
799 green). In Leporids, *RIPK3* was lost as a result of a shared insertion (+G) in the third exon  
800 that resulted in the appearance of several premature stop codons. **B)** A point mutation (C

801 to T) in all the studied cetacean species indicates that MLKL inactivation occurred in  
802 Cetacea steam lineage. Moreover, 9 out of the 11 studied species (excluding *B.*  
803 *acutorostrata* and *M. Monoceros*) lost exon 2, 3, 4 and 5 throughout evolution (represented  
804 by faint yellow). Premature stop codons are represented by an asterisk (\*).

805 **Fig. 4 Gene synteny of the genome regions containing MLKL gene in different**  
806 **mammals.** Genomic regions containing the *MLKL* gene or its flanking genes in *H. sapiens*,  
807 *M. musculus*, *O. curzoniae*, *O. cuniculus*, *P. vampyrus*, *C. lupus* and *B. taurus*. Horizontal  
808 lines indicate chromosome fragments and coloured arrows identify genes and their  
809 orientation in the genome. Orthologous genes are indicated in the same colour and their  
810 names are indicated above/below. Black arrows indicate the presence of pseudogenes.  
811 Abbreviations: RFWD3, ring finger and WD repeat domain 3; MLKL, mixed-lineage kinase  
812 domain like; FA2H, fatty acid 2-hydroxylase; GLG1, golgi glycoprotein 1; WDR59, WD  
813 repeat domain 59; *TMPOP2*, thymopietin pseudogene; *GM6014*, ubiquitin-40S ribosomal  
814 protein S27a pseudogene; *LOC788457*, translationally-controlled 1 pseudogene.

815 **Fig. 5 Protein sequence alignment of E3L proteins. A)** Schematic diagram of VACV E3  
816 protein binding domains: yellow box represents the zNA-BD and blue box represents the  
817 dsRNA-BD. The same color scheme is used in B and C. **B)** E3L homologues from 11  
818 poxviruses (VACV E3, Cowpoxvirus (CPXV) 069, Tateropoxvirus (TATV) 060, Yaba  
819 monkey tumor virus (YMTV) 034, swinepoxvirus (SWPV) 34L, Deerpoxvirus (DPV) 042,  
820 Sheeppoxvirus (SPPV) 034, Monkeypoxvirus (MPXV) F3, Myxoma virus (MYXV) M029  
821 and Cetaceanpoxvirus (CePV) CePV-TA-20 and 21) were used to perform a schematic  
822 alignment using COBALT program from the NCBI platform. Length of each E3L  
823 homologue as well as their identity to VACV E3 proteins are shown in the column to the  
824 right. **C)** Amino acid sequence comparison of 11 different members of the E3L family  
825 including VACV E3, TATV 060, YMTV 034, SWPV 34L, DPV 042, SSPPV 034, MPXV F3  
826 and MYXV M029 and CePV-TA 20 and 21. Conserved areas known to bind to zNA are  
827 shown in grey boxes.

## 828 **Supporting information**

829 **S. Appendix 1** Accession numbers for *RIPK1*, *RIPK3* and *MLKL* genes found in different  
830 mammalian lineages.

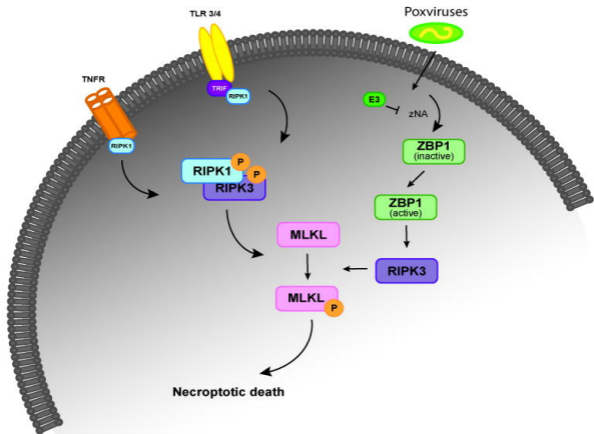
831 **S. Appendix 2** Accession numbers for *RIPK1*, *RIPK3* obtained from different Leporid  
832 samples.

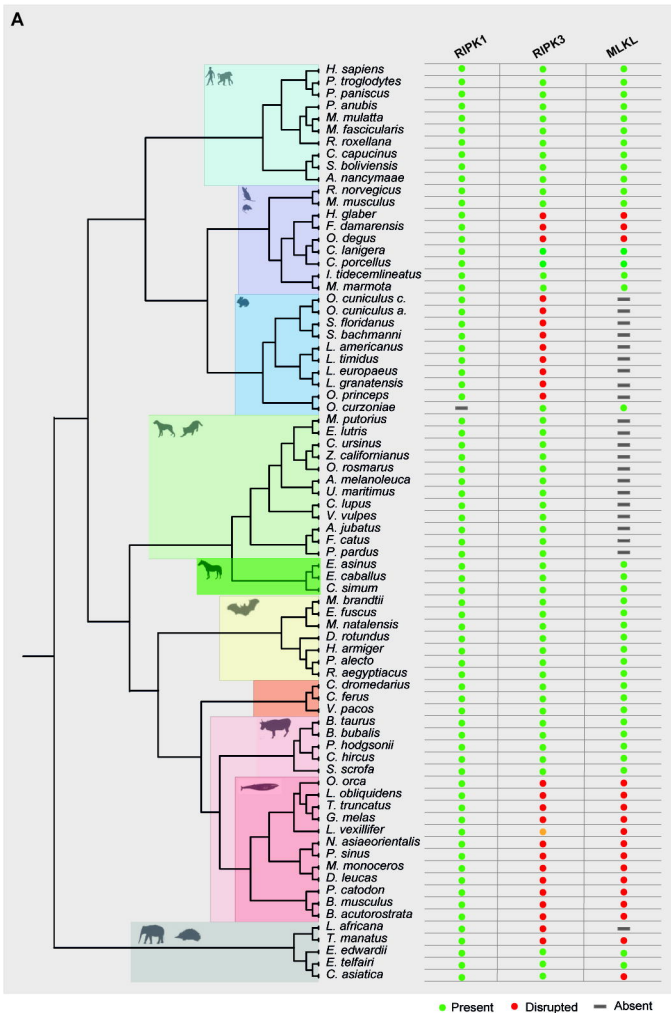
833 **S. Appendix 3** Phylogenetic analysis for RIPK1, RIPK3 and MLKL proteins from different  
834 mammalian lineages.

835 **S. Appendix 4** Positive and negative selection analyses for RIPK1 protein.

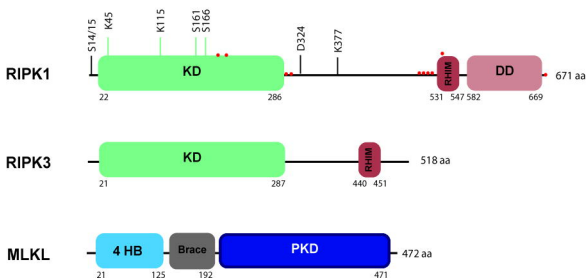
836 **S. Appendix 5** RIPK3 and MLKL protein alignment from species from rodent and  
837 afrotheria lineages.

838 **S. Appendix 6** Tables identifying RIPK3 and MLKL mutations and premature stop codons  
839 in Cetacea order.

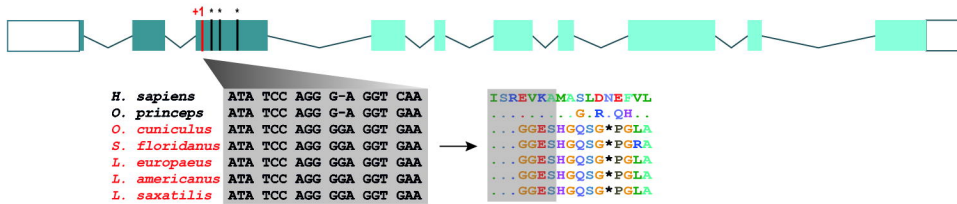




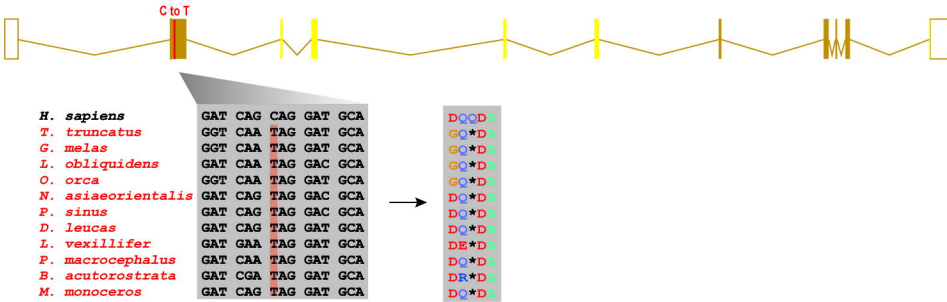
**B**



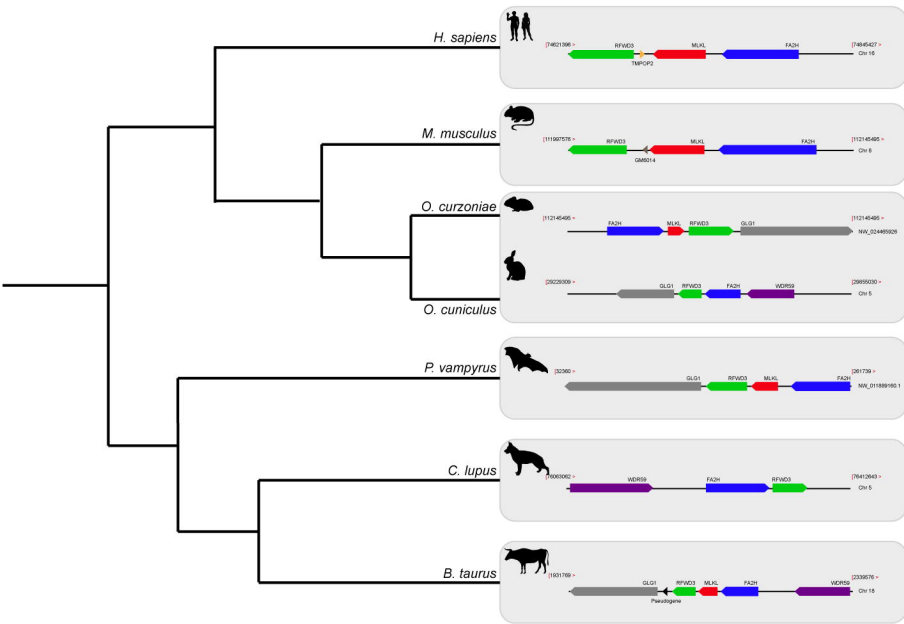
A



B



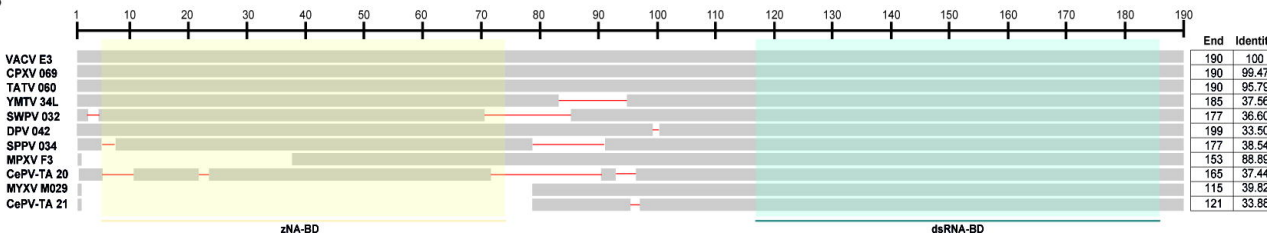




**A**



**B**



**C**

